Modification of three-dimensional transition in the wake of a rotationally oscillating cylinder

DAVID LO JACONO[1,2,3]†, **JUSTIN S. LEONTINI**[3],
MARK C. THOMPSON[3] **AND JOHN SHERIDAN**[3]

[1]Université de Toulouse; INPT, UPS; IMFT (Institut de Mécanique des Fluides de Toulouse);
Allée Camille Soula, F-31400 Toulouse, France

[2]CNRS; IMFT; F-31400 Toulouse, France

[3]Fluids Laboratory for Aeronautical and Industrial Research (FLAIR), Department of Mechanical
and Aerospace Engineering, Monash University, Melbourne, Victoria 3800, Australia

A study of the flow past an oscillatory rotating cylinder has been conducted, where the frequency of oscillation has been matched to the natural frequency of the vortex street generated in the wake of a stationary cylinder, at Reynolds number 300. The focus is on the wake transition to three-dimensional flow and, in particular, the changes induced in this transition by the addition of the oscillatory rotation. Using Floquet stability analysis, it is found that the fine-scale three-dimensional mode that typically dominates the wake at a Reynolds number beyond that at the second transition to three-dimensional flow (referred to as mode B) is suppressed for amplitudes of rotation beyond a critical amplitude, in agreement with past studies. However, the rotation does not suppress the development of three-dimensionality completely, as other modes are discovered that would lead to three-dimensional flow. In particular, the longer-wavelength mode that leads the three-dimensional transition in the wake of a stationary cylinder (referred to as mode A) is left essentially unaffected at low amplitudes of rotation. At higher amplitudes of oscillation, mode A is also suppressed as the two-dimensional near wake changes in character from a single- to a double-row wake; however, another mode is predicted to render the flow three-dimensional, dubbed mode D (for double row). This mode has the same spatio-temporal symmetries as mode A.

Key words: instability, instability control, vortex streets

1. Introduction

The wake of a circular cylinder immersed in a free stream goes through a series of well-documented transitions with increasing Reynolds number $Re = Ud/\nu$, where U is the free-stream velocity, d is the cylinder diameter and ν is the kinematic viscosity. The first of these transitions occurs at $Re \simeq 47$ (Provansal, Mathis & Boyer 1987). This is the primary Hopf bifurcation, where the wake transits from a steady flow to periodic vortex shedding, forming the Kármán–Bénard vortex street. The second transition occurs at $Re \simeq 190$ (Barkley & Henderson 1996; Williamson 1996) when this vortex street becomes three-dimensional.

† Email address for correspondence: david.lojacono@eng.monash.edu.au

A number of researchers have focused their attention on the control of the primary bifurcation; in the context of the study presented here, the results of Thiria, Goujon-Durand & Wesfreid (2006) and Thiria & Wesfreid (2007) have shown that a rotational oscillation can effectively suppress the global mode leading to synchronized vortex shedding, depending on the frequency of oscillation.

However, it is the secondary bifurcation which really marks the beginning of the route to turbulence in the wake. A large body of work has been completed, isolating and identifying the modes involved in this transition to three-dimensional flow. The seminal work of Williamson (1988) was the first to identify two distinct three-dimensional modes (modes A and B) occurring in the cylinder wake. The wake initially becomes unstable to mode A (Williamson 1988), which appears to be driven by an elliptic instability of the vortex cores (Leweke & Williamson 1998b; Thompson, Leweke & Williamson 2001; Julien, Lasheras & Chomaz 2003), although there has been debate about associating such complex transitions with simple generic instability mechanisms (Barkley & Henderson 1996; Henderson 1997). A second mode, mode B, has been shown to become linearly unstable at $Re \simeq 260$ (Barkley & Henderson 1996); however, the presence of mode A is destabilizing on mode B (Barkley, Tuckerman & Golubitsky 2000; Sheard, Thompson & Hourigan 2003a), and the first sign of mode B is observed experimentally at Reynolds numbers closer to $Re = 230$ (Williamson 1996). Mode B eventually becomes dominant, with streamwise vortical structures on the scale of this mode still present at $Re = 1000$ (Wu *et al.* 1996) and beyond. A third mode exists, dubbed mode QP, due to the fact that it is quasi-periodic. It becomes linearly unstable at $Re = 377$ (Blackburn & Lopez 2003). However, due to the presence of mode A and B, clear identification of the influence of mode QP during experiments has proven to be elusive. In fact, the wake appears to be essentially chaotic for Reynolds numbers not much greater than 300 (Henderson 1997).

The group theory analysis of Marques, Lopez & Blackburn (2004) and Blackburn, Marques & Lopez (2005) showed that certain symmetry properties need to be respected by the three-dimensional modes that bifurcate from the two-dimensional Kármán–Bénard vortex street. Only three generic bifurcation symmetries can exist; these correspond to the spatio-temporal symmetries of modes A, B and QP.

However, the aforementioned analysis places no restrictions on the order in which these modes can become unstable. Henderson (1997) and Karniadakis & Triantafyllou (1992) showed that varying the spanwise extent of the cylinder in a spatially periodic simulation could vary the route to turbulence from a period-doubling cascade led by mode B, to a transition to spatio-temporal chaos led by mode A. This implies that suppression of one mode can influence the route to turbulence.

Leontini, Thompson & Hourigan (2007) showed that a transverse oscillation of the cylinder close to the natural vortex shedding frequency could result in mode B naturally leading the three-dimensional transition. In that case, the transverse oscillation effectively suppressed mode A by influencing the size of the vortex cores. Analogous to this, for elongated elliptical leading-edge plates, Ryan, Thompson & Hourigan (2005) showed that a mode with the same spatio-temporal symmetry as mode B undergoes transition before mode A, once the aspect ratio of the plate becomes sufficiently large.

This raises the question: can the same control be effected on mode B? This is an important question to answer, due to the dominant role that mode B plays in the wake dynamics over a wide range of Re. The results of Poncet (2002) suggest a rotational oscillation can achieve this goal.

The results presented in this paper show that a rotational oscillation, at the natural shedding frequency, effectively suppresses mode B at $Re = 300$, confirming the result

of Poncet (2002). However, the oscillation has a lesser effect on the other modes present. This is shown using Floquet stability analysis. As well as this direct effect on mode B, an interesting side effect is that at higher rotational oscillation amplitudes, a new mode appears with the same symmetries as the 'classic' mode A, but with a shorter characteristic wavelength. This new mode appears to be a kind of higher spatial resonance, that obeys the symmetry laws of the analysis of Marques *et al.* (2004). This suppression of mode growth, and the emergence of a new mode, has been quantified, and the structure of the new mode is presented.

2. Numerical formulation

2.1. *Flow field calculation*

The three-dimensional stability of the wake is determined by whether, at any particular Reynolds number, three-dimensional perturbations grow or decay on an imposed two-dimensional wake (base) flow. The base flows for the present study were calculated by solving the incompressible, time-dependent Navier–Stokes equations. For the perturbation fields, the equations solved were formed by taking these same equations, splitting the velocity and pressure fields into base and perturbation components, subtracting the original equations for the base flow, and linearizing the result.

The discretization method employed was a spectral element method, using fifth-order Lagrange polynomials as shape and weighting functions over each element, associated with Gauss–Lobatto–Legendre quadrature points for efficient calculation of the required integrals. The time integration was executed using a three-step splitting scheme (Karniadakis, Israeli & Orszag 1991; Thompson *et al.* 2006*a*), employing an explicit third-order Adams–Bashforth scheme for the convective substep, a centred scheme for the pressure correction term and an implicit Crank–Nicholson method with the theta-correction (Canuto *et al.* 1990) for the diffusion term. First-order pressure boundary conditions result in second-order time accuracy for the predicted velocity field.

A computational domain extending $25d$ downstream, $15d$ upstream and $15d$ to either side of the cylinder was split into 518 elements, the majority of which were concentrated in the boundary layer and wake regions. The resolution, element distribution and domain size are consistent with those used successfully in previous similar studies (Thompson, Hourigan & Sheridan 1996; Thompson *et al.* 2001; Leontini *et al.* 2007).

Free-stream (Dirichlet) boundary conditions were enforced at the upstream and lateral boundaries, while a Neumann-type boundary condition was employed at the outlet, which is sufficient for vortices to freely exit the domain at the Reynolds numbers under consideration in this paper. At the cylinder surface, a time-dependent Dirichlet condition was utilized that varied sinusoidally in time according to a driven rotational oscillation,

$$\theta = A_\theta \sin(2\pi f_\theta t), \qquad (2.1)$$

where A_θ is the amplitude of rotation in radians, and the frequency (f_θ) and time (t) are non-dimensional quantities using U and d. The frequency of oscillation was selected to match the Strouhal frequency for a fixed cylinder at the same Reynolds number according to the functional fit given by Williamson & Brown (1998), which returns a frequency of $f_\theta = 0.210453$ for $Re = 300$. This tangential velocity at the cylinder boundary needs to be taken into account with the implementation of the pressure boundary condition to maintain second-order accuracy of the velocity field.

The description of the methodology is purposefully brief because of descriptions given in previous papers. Details of the method in general can be found in

Karniadakis & Sherwin (2005), and details of the implementation used here in Thompson *et al.* (1996). The code employed has been well proven for use in bluff body problems and Floquet stability analysis (Sheard, Thompson & Hourigan 2003*b*; Ryan *et al.* 2005; Leontini *et al.* 2007).

2.2. *Floquet stability analysis*

Floquet stability analysis is a linear method designed to deduce the stability of periodic solutions. Here, it is used to analyse the stability of a periodic two-dimensional flow to three-dimensional perturbations. The stability is deduced by calculating the Floquet multiplier μ which can be thought of as the ratio of growth in amplitude of a perturbation from one period to the next, for a perturbation of a given spanwise wavelength, λ. If this ratio is such that $|\mu| > 1$, the perturbation grows each period, and the two-dimensional base flow is said to be unstable. Conversely, if $|\mu| < 1$, the perturbation decays each period, and will eventually die away, meaning the base flow is stable. Generally, this relies on the fact that a random perturbation of a given wavelength can be decomposed into a summation of eigen or Floquet modes, each of which grow or decay at a certain rate. It is the fastest growing or slowest decaying Floquet mode – the dominant mode – which dominates asymptotically with time. That is, after a long time, a perturbation decays to the dominant Floquet mode, with the size of the Floquet multiplier relative to unity determining the stability of the base flow. Details of the formulation can be found in Barkley & Henderson (1996), Ryan *et al.* (2005) and Leontini *et al.* (2007).

The code employed has been used previously for Floquet stability analysis, employing a power method to resolve the most dominant Floquet mode (and the magnitude of the largest Floquet multiplier). While this method can be effective when there is a single clearly dominant mode, it does not allow for the separation of two or more modes that may have equal-amplitude Floquet multipliers for a given spanwise wavelength. This happens if the dominant mode Floquet multiplier is complex, in which case it occurs as a complex pair, in order to enable real perturbation fields to be constructed. Therefore, a Krylov subspace method has been implemented, using an Arnoldi decomposition to resolve the full complex Floquet multipliers. The implementation used here is essentially the same as that used in Blackburn & Lopez (2003).

The use of this implementation allows modes with similar growth rates to be effectively separated, and the resolution of the real and complex components of the Floquet multipliers associated with each mode. It should be noted that for this study, the amplitude of the perturbation fields only within $10d$ of the cylinder are allowed to contribute to the computed dominant Floquet multipliers, ensuring the Floquet multipliers are computed on a region of the base flow that is periodic (or close to periodic). Further downstream the wake is not necessarily periodic, or at least not with the same frequency as the near wake due to vortex pairing and secondary instabilities (Williamson & Prasad 1993; Johnson, Thompson & Hourigan 2004).

It is strictly true that Floquet stability analysis requires the base flow to be periodic. However, even if the flow is only approximately periodic, a linear stability analysis can provide valuable information about the nature of the modes that lead to the flow becoming three-dimensional. The choice of limiting the downstream domain of the perturbation field to $10d$ provided such an approximately periodic base flow for all calculations for this study. Johnson *et al.* (2004) showed by Fourier analysis for similar low-Reynolds-number wakes that upstream of the vortex pairing/remerging, there is virtually no frequency content apart from the Strouhal frequency, consistent
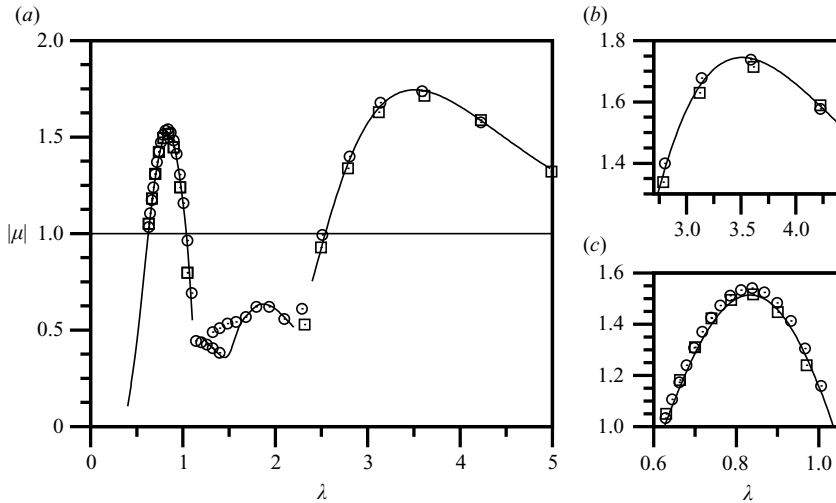
FIGURE 1. Moduli of the Floquet multipliers μ versus spanwise wavelength λ (spanwise wavenumber $k = 2\pi/\lambda$) for the three-dimensional instability modes of the two-dimensional wake of a circular cylinder at $Re = 280$. The current results (solid line) are compared with those from Barkley & Henderson (1996) (open squares) and Blackburn & Lopez (2003) (open circles).

with the picture that pairing has little effect on the upstream flow. Thus, this seems a reasonable approach provided the perturbation field grows predominantly only within the near wake. The veracity of this assumption will be examined in the results section.

2.3. *Validation*

For validation of the methods employed, the grid resolution, the domain size and the Floquet stability analysis, the wake transitions for a fixed cylinder in a uniform flow were analysed. Floquet multipliers were calculated for a range of wavelengths at $Re = 280$. The results are compared with those from Barkley & Henderson (1996) and Blackburn & Lopez (2003) in figure 1. The match is excellent, with $|\mu|$ and λ at the peaks of the curves for each mode faithfully reproduced.

These results validate that the method is correctly implemented, and that the mesh resolution is adequate to resolve the physics of the problem. Note, as mentioned before, similar meshes, mesh resolutions and domain sizes have been used previously for similar studies.

To further validate the choice of the current computational resolution at the Reynolds number of the current study, a further resolution studied was performed, in which the order (p) of the element interpolating polynomials was varied. This study indicates that the choice of polynomial order selected for the simulations ($p = 6$) resolves the mode B multiplier to within about 2 % at $Re = 300$.

3. Results and discussion
3.1. *Effect of the amplitude of rotation on the base flow*

Figure 2 depicts contours of vorticity of the two-dimensional base flow past a rotationally oscillating cylinder at $Re = 300$. For these wakes, there are three downstream stages; single row, double row and a long-wavelength wake. Initially, by increasing the amplitude of rotation, the distances downstream where the double-row
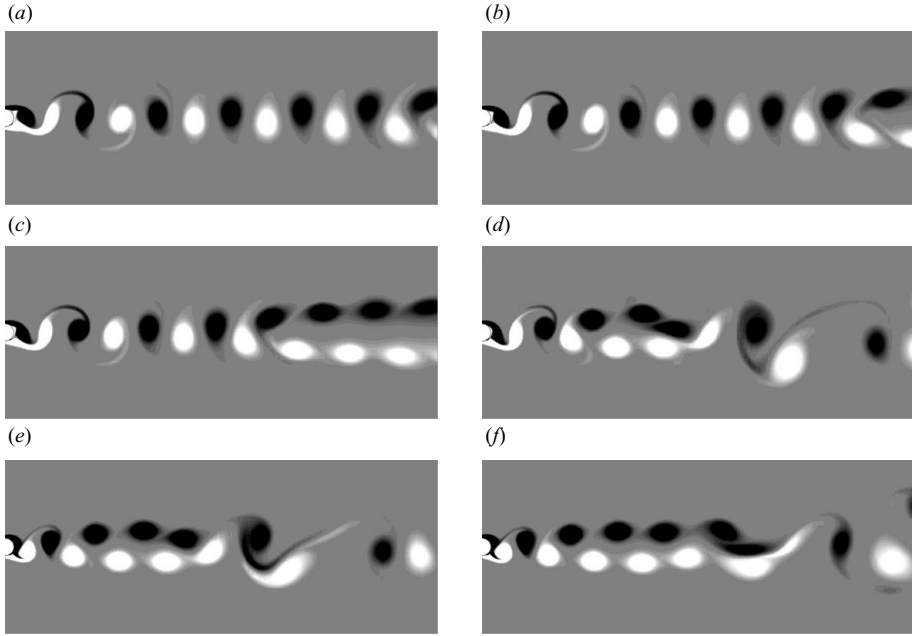
FIGURE 2. Contours of vorticity of the two-dimensional base flow past a cylinder undergoing several amplitudes of rotation at $Re = 300$. The flow is from left to right. The amplitudes of the imposed rotation are expressed in radians. Amplitude of rotation (A_θ) increases as: $A_\theta = 0$, 0.20, 0.40, 0.60, 0.80, 1.00 from (a) to (f), respectively. All the images are taken at $\theta = 0$. White (black) represents positive (negative) vorticity. For all the cases considered the near wake was synchronized to the forcing frequency.

configuration and the long-wavelength configuration begin are decreased ($A_\theta < 0.60$). Conversely, as the amplitude of rotation is further increased, the distance downstream where the long-wavelength wake configuration begins is increased. For all the cases considered, the near wake (up to at least $10d$) was synchronized to the forcing frequency. The forcing frequency was the Strouhal frequency for a fixed cylinder at the same Reynolds number according to the relationship of Williamson & Brown (1998). Similar effects on the wake configuration for a different forcing mechanism (e.g. forced crossflow oscillation) can be found in Leontini et al. (2006). For forcing amplitude $A_\theta > 1$ the base flow was not periodic on any sub-domain, precluding any Floquet analysis.

3.2. Effect of the amplitude of rotation on the different modes

Figure 3 shows the moduli of the Floquet multipliers μ versus spanwise wavelength λ for the three-dimensional instability modes at $Re = 300$. The control case of the fixed cylinder is shown in figure 3(a), and the results are certainly consistent with those at $Re = 280$ shown in figure 1.

Figure 3 shows the dependence of the growth rate for each of the modes on A_θ. Figure 3 also shows, indirectly, the dependence of the characteristic wavelength for each mode (i.e. the wavelength at which the maximum growth rate occurs, $\lambda_{char} = \lambda(|\mu|_{max})$) on A_θ. Of note, comparing figures 3(a) and 3(b) shows that as the amplitude of rotation is increased from the control case of $A_\theta = 0$–0.2, the growth rates of the modes are varied, but the same classic modes are present. However, increasing the amplitude of rotation to $A_\theta = 0.4$ sees mode B diminish to the point
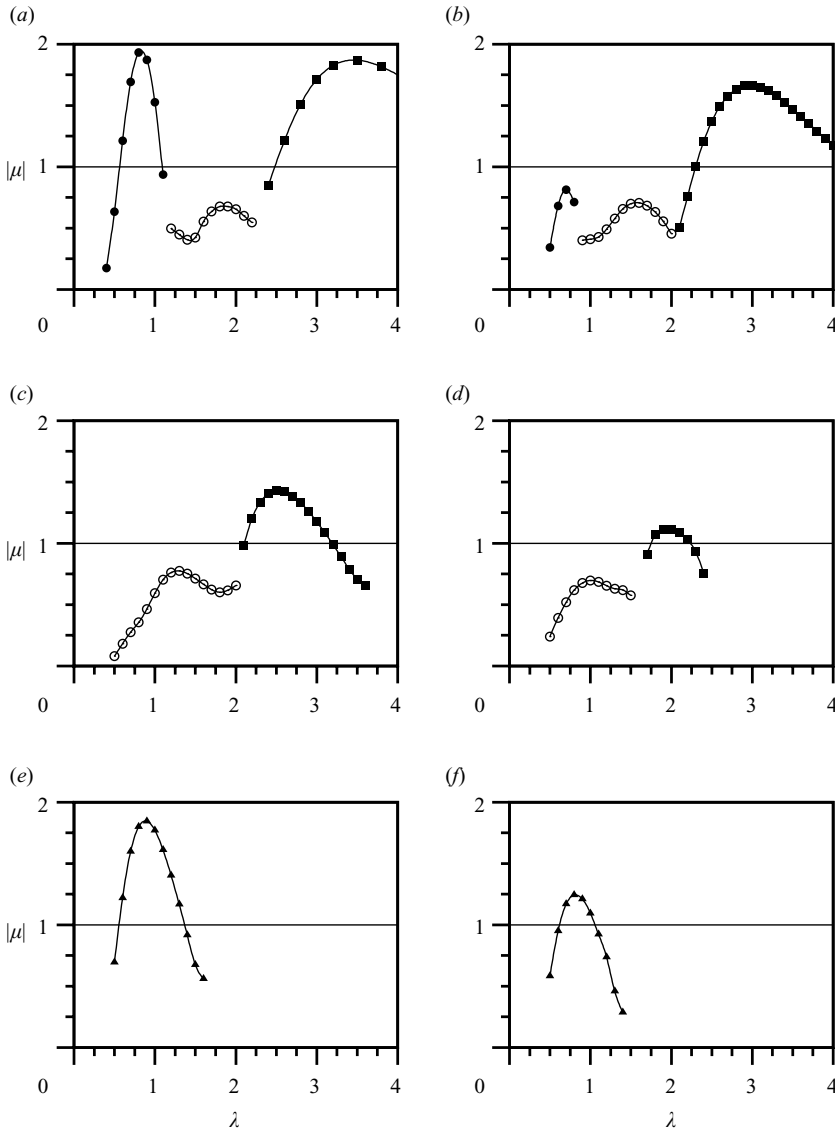
FIGURE 3. Moduli of the Floquet multipliers μ versus spanwise wavelength λ for the three-dimensional instability modes of the two-dimensional wake of a rotationally oscillating circular cylinder at $Re = 300$. The amplitude of rotation spans the range $0 < A_\theta < 1$. Amplitude of rotation (A_θ) increases as: $A_\theta = 0$, 0.20, 0.40, 0.60, 0.80, 1.00 from (a) to (f), respectively. Filled symbols (open symbols) represent modes with purely real (complex) Floquet multipliers. Filled squares represent mode A; filled circles represent mode B; filled triangles represent mode D; open circles represent mode QP. Oscillation suppresses mode B but does not suppress all three-dimensional instabilities.

where it cannot be resolved, leaving only modes A and QP. Further increasing the amplitude of rotation to $A_\theta = 0.8$ sees both of these modes also disappear, and a new mode (dubbed mode D) arise. Only mode D is resolved for $A_\theta \geqslant 0.8$, and hence only the curve representing this mode is shown in figures 3(e) and 3(f).

Because mode D forms on a base flow that is not strictly periodic, the approach adopted to obtain Floquet multipliers (where only the near wake is considered in
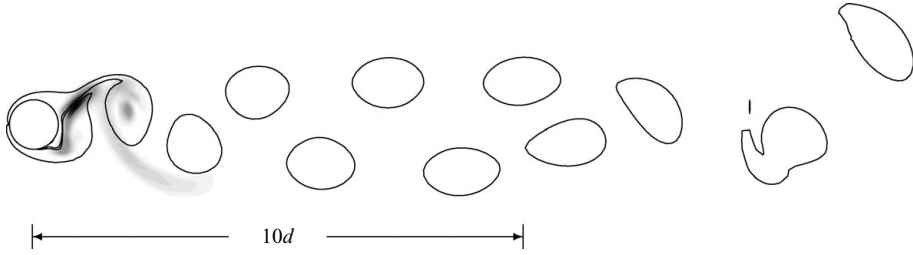
FIGURE 4. Perturbation energy field for mode D for $A_\theta = 0.8$ and $\lambda/d = 0.9$, showing that the perturbation field is of high amplitude mainly in the region prior to pairing. Greyscale contours show perturbation energy, solid lines show base flow vorticity at ± 0.5.
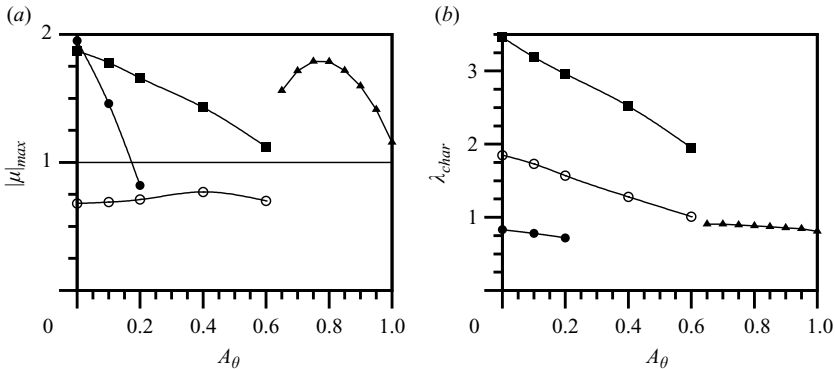

FIGURE 5. (*a*) The maximum magnitude of the Floquet multiplier $|\mu|_{max}$ as a function of the amplitude of oscillation A_θ for each of the four modes described. (*b*) The characteristic wavelength λ_{char} as a function of the amplitude of oscillation A_θ for each of the four modes described. The Reynolds number is $Re = 300$. For both plots, filled squares represent mode A, filled circles represent mode B, open circles represent mode QP and filled triangles represent mode D.

the calculation of the growth rate) perhaps requires further justification. Importantly, figure 4 shows that the perturbation field is mainly restricted to the near wake, prior to pairing. If the full domain is used to determine the (approximate) dominant Floquet multiplier using Arnoldi decomposition with the Krylov subspace approach, it is found to be constant to within less than $\pm 1\%$ compared to the case of truncating the domain at $10d$, and therefore agrees with the approach using the truncated domain.

To ensure consistency, a similar validation study was carried out for mode A at $A_\theta = 0.6$. In this case, the approximate dominant Floquet multiplier was calculated over: the full domain; the domain truncated at $10d$; the domain truncated at $6d$. The multipliers calculated on the whole domain and on the domain truncated at $6d$ were then compared to the multiplier calculated on the domain truncated at $10d$. In both cases, the variation was within $\pm 5\%$. It should also be noted that the growth rate and characteristic wavelength for mode A vary smoothly with A_θ all the way to $A_\theta = 0.6$, as shown in figure 5. These facts provide a high level of confidence in the truncated domain method.

These results shown in figure 3 are summarized in figure 5(*a*) for the maximum growth rates and in figure 5(*b*) for the associated characteristic wavelengths. Figure 5(*a*) demonstrates the rapid suppression of mode B with increasing A_θ, and that mode A is suppressed, but not as effectively. The growth rate of mode QP is
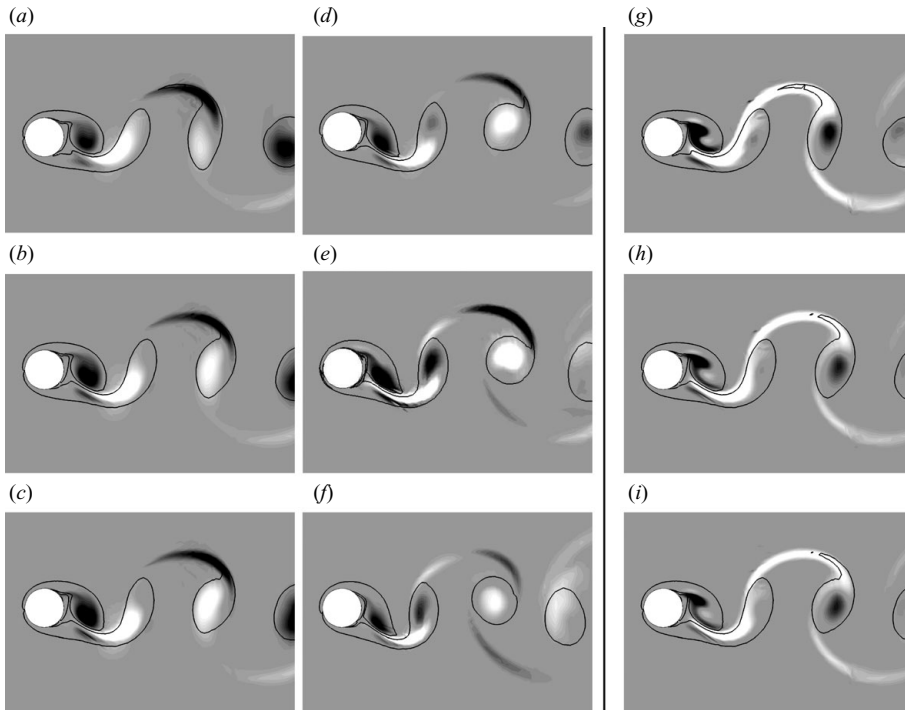
FIGURE 6. Streamwise perturbation vorticity for (*a*) Mode A when $\lambda = 3.5$ ($k = 1.80$) at $A_\theta = 0$; (*b*) Mode A when $\lambda = 3.2$ ($k = 1.96$) at $A_\theta = 0.1$; (*c*) Mode A when $\lambda = 3.0$ ($k = 2.09$) at $A_\theta = 0.2$; (*d*) Mode A when $\lambda = 2.5$ ($k = 2.51$) at $A_\theta = 0.4$; (*e*) Mode A when $\lambda = 2.2$ ($k = 2.85$) at $A_\theta = 0.5$; (*f*) Mode A when $\lambda = 1.9$ ($k = 3.31$) at $A_\theta = 0.6$; (*g*) Mode B when $\lambda = 0.8$ ($k = 7.85$) at $A_\theta = 0$; (*h*) Mode B when $\lambda = 0.8$ ($k = 7.85$) at $A_\theta = 0.1$; (*i*) Mode B when $\lambda = 0.7$ ($k = 8.97$) at $A_\theta = 0.2$. White (black) represents positive (negative) streamwise vorticity. Solid lines represent base flow vorticity at $\omega = \pm 1$. The basic structures of the modes are unaffected by the forcing amplitude.

relatively unaffected by the oscillation, and the amplitude of the multipliers remains less than unity for the entire range of rotational amplitudes at this Reynolds number. Figure 5(*b*) demonstrates that the amplitude of oscillation has a marked effect on the characteristic wavelength of modes A and QP, with almost a 50 % reduction in the mode A wavelength as the rotational amplitude is increased to 0.6. This presumably reflects the decreasing length scales in the wake as the shed vortices become more compact. Both plots show that for $A_\theta \geqslant 0.65$, only the new mode can be resolved, and it has a Floquet multiplier greater than unity. It is proposed to call this mode D, because it occurs when the rotational oscillation is sufficiently strong to force the occurrence of a double-row vortex street almost from the beginning of the wake. In effect, this also explains the seemingly sudden change in the three-dimensional wake stability between $A_\theta < 0.6$ and $A_\theta > 0.8$. This is consistent with the near wake changing from a single-row to a double-row wake as the two-dimensional vortices grow in strength because of the increased vorticity flux into the forming vortices caused by the rotational oscillation.

Figure 6 presents the streamwise vorticity of the three-dimensional modes A and B for increasing rotational amplitude. These modes for $A_\theta = 0$ are identical to those of Barkley & Henderson (1996) and Blackburn *et al.* (2005). From inspection of figure 6 it is clear that the structure of these modes is essentially unaffected by the rotational oscillation.
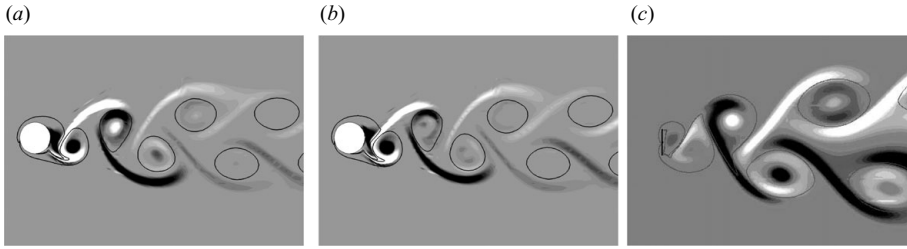
(*a*)   (*b*)   (*c*)

FIGURE 7. Contours of streamwise perturbation vorticity for (*a*) $\lambda = 0.9$ ($k = 6.98$) mode D at $A_\theta = 0.8$; (*b*) $\lambda = 0.8$ ($k = 7.85$) mode D at $A_\theta = 1.0$; (*c*) flat plate transition mode. White (black) represents positive (negative) streamwise vorticity. Solid lines represent base flow vorticity at $\omega = \pm 1$. The general mode structure is unaffected by the forcing amplitude. This previously undocumented mode possesses the same symmetries as mode A, yet has a finer spatial scale. Some similarities on the mode topology also occurs for a normal flat plate wake (*c*), which also has a double-row vortex street. In the latter case $\lambda = 2$ plate heights and $Re = 126$.

Mode A presents a spatio-temporal symmetry (spatial reflection and half-period evolution), $(U, V, W)(x, y, t) = (U, -V, W)(x, -y, t + T/2)$. It has been proposed that the underlying mechanism is a cooperative elliptic instability (Thompson *et al.* 2001; Leweke & Williamson 1998*a*,*b*; Julien *et al.* 2003) of the vortex cores in the near wake. Mode B breaks the latter symmetry, instead obeying $(U, V, W)(x, y, t) = (U, V, -W)(x, -y, t + T/2)$ as can be seen in figure 6(*g*). The dominant physical cause of mode B has been proposed to be due to various instability types such as a hyperbolic instability of the braids (Leweke & Williamson 1998*a*) or a centrifugal instability of the forming vortex cores amplified in the braids (Ryan *et al.* 2005).

3.3. *Mode D*

Figure 7 presents the previously unreported mode associated with high amplitudes of rotation. This mode possesses the same symmetries as mode A, however it has additional features on a shorter length scale, notably in the cores of the vortices.

A mode with some similar features to mode D occurs for a flat plate wake (Thompson *et al.* 2006*b*), and this is represented in figure 7(*c*). This flow also has the double-row vortex street due to the stronger and more compact wake vortices. The figure represents the mode behind a flat plate at $Re = 126$.

From the figure it is clear that this flat plate mode and mode D share some of the same basic shape structure and spatio-temporal symmetries. However, a close inspection of the mode behind the flat plate reveals that the initial growth is located between the second and third wake vortices, whereas mode D (as shown in figure 8) grows predominantly between the first and second vortices. Despite this difference, it is possible that the underlying instability mechanism for the two modes is the same. The local flow in the region of high growth for both modes is at least qualitatively similar; in both cases the modes are most energetic in the region of high strain between two wake vortices. Further study is required to fully compare these two modes, and to try to identify the physical mechanism that causes them.

Figure 8 shows the variation of the near wake topology with increasing A_θ. The longitudinal spacing of the vortices is reduced as the rotational amplitude is increased. The boundary layer at the rear of the cylinder becomes much thinner as A_θ is increased. However, mode D grows predominantly in the region between the first and second wake vortices, approximately $1d$ away the centre of the cylinder. This suggests
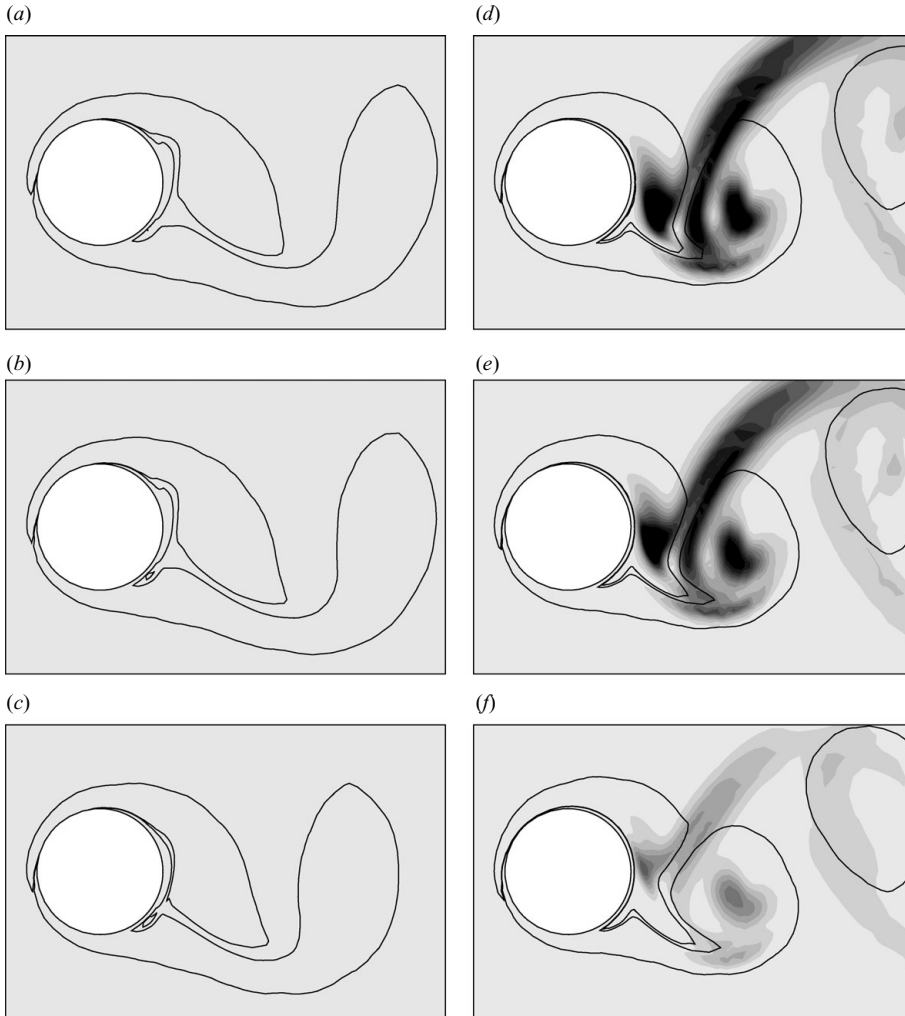
FIGURE 8. Variation of the near wake topology with increasing A_θ: 0.4, 0.5, 0.6, 0.7, 0.8, 1.0 from (*a*) to (*f*), respectively. Represented are the base flow vorticity (solid lines) and the perturbation energy for mode D (black and white contours). Note that mode D could only be resolved for $A_\theta \geqslant 0.65$. Images (*d*), (*e*) and (*f*) show that mode D is the most energetic in the area between the first and second wake vortices.

that the inter-vortex spacing is the critical topological factor concerning the rapid destabilization of mode D as A_θ is increased beyond 0.65.

3.4. *Stabilization of mode B*

Of the three-dimensional modes described, mode B is the most heavily influenced with regard to its growth rate by the rotational oscillation amplitude. This is clear from inspection of figure 5(*a*), despite the fact that the base flow is almost unaffected in basic structure in the near wake for small amplitudes of rotation. This is most likely due to the fact that mode B is an instability of the braid shear layer between the forming and shed vortices (see figure 7*g*) or at least relies on amplification in the braids. While the wake structure appears essentially the same at small amplitudes of oscillation, it is clear from the sequence in figure 2, and the sequence in figure 8,

A_θ	λ	$\lvert\mu\rvert^2$	$\mathcal{D}/\mathcal{E}_I$	$\mathcal{P}/\mathcal{E}_I$	$\mathcal{D}/\mathcal{E}_I + \mathcal{P}/\mathcal{E}_I$	$\lvert\mathcal{D}/\mathcal{P}\rvert$
0	0.83	4.00	−8.97	11.97	3.00	0.75
0.10	0.80	2.64	−7.76	9.40	1.64	0.83
0.20	0.74	0.99	−4.82	4.81	−0.01	1.00

TABLE 1. Perturbation energy dissipation ($\mathcal{D}/\mathcal{E}_I$) and production ($\mathcal{P}/\mathcal{E}_I$) over a cycle of oscillation (both scaled by the initial perturbation energy $\mathcal{E}_I$) over a range of amplitude of rotation for mode B. Note that $\lvert\mu^2\rvert$ gives the energy growth over the period. With increasing amplitude, the relative importance of the dissipation increases.

that rotational oscillation does make the vortices increasingly compact and reduces the wake formation length. Thus, an effect of the oscillation is to reduce the length scale of the vortex cores of the base flow and, in turn, the braid length scale. This is important because whether an instability mode decays or grows depends on the balance between the inviscid growth mechanism and viscous damping. For example, mode A growth depends on whether an elliptic instability of the cores can overcome viscous damping at a particular spanwise wavelength linked to the core size (Leweke & Williamson 1998b). These two effects can be considered linearly additive (e.g. see Landman & Saffman 1987; Leweke & Williamson 1998b). Viscous damping depends on the reciprocal of the square of the selected wavelength (Landman & Saffman 1987). This can be qualitatively understood because the viscous term in the Navier–Stokes equations depends on the local curvature of the velocity field. Thus, reducing the length scales of base flow features such as the braid shear layer, which in turn determine the selected wavelengths of instability modes, will have a much greater influence on shorter wavelength instabilities; so mode B will be damped more efficiently than mode A as the oscillation amplitude is increased.

Support for this hypothesis can be found by looking at the perturbation energy balance. Integrating the perturbation energy over the entire domain for a cycle gives

$$\Delta\mathcal{E} = -\int_T \int_\Omega \hat{u}_i \hat{u}_j \frac{\partial U_i}{\partial x_j}\,\mathrm{d}\Omega\,\mathrm{d}\tau - \frac{1}{Re}\int_T \int_\Omega \frac{\partial \hat{u}_i}{\partial x_j}\frac{\partial \hat{u}_i}{\partial x_j}\,\mathrm{d}\Omega\,\mathrm{d}\tau, \qquad (3.1)$$

where T defines a period of oscillation, Ω is the computational domain, $\hat{u}_i$ is the perturbation velocity field and U_i is the base velocity field. Here, $\Delta\mathcal{E}$ is the energy change, and the first and second terms on the right-hand side are the production ($\mathcal{P}$) and the dissipation ($\mathcal{D}$), respectively. These quantities have been calculated over a range of amplitudes for mode B, for the fastest growing wavelength. The results are presented in table 1. The results indicate that as the rotation rate increases both the production and dissipation decrease strongly, but that dissipation decreases less slowly. Notice that the change in the preferred wavelength from $A_\theta = 0.2$–0 is approximately 12 %. Given the dissipation varies with the square of the length scale, this indicates that the percentage change in the dissipation between these two cases should be $2 \times 12 = 24$ %, consistent with the observed change of 25 % shown in the last column of the table. Thus, the suppression of mode B appears to be due to the substantial reduction in the controlling length scale as the rotation rate is increased.

4. Conclusions

A study of the flow past a rotationally oscillating cylinder was undertaken, where the frequency of oscillation was matched to the natural vortex-shedding frequency from

a fixed cylinder at the same Reynolds number. It was found that, for $Re = 300$, the primary frequency of the near wake remained synchronized to the driving frequency for amplitudes of rotational oscillation where $A_\theta \leqslant 1$. The effect of rotational oscillation on the two-dimensional base flow is substantial, changing the wake from a single-row to a double-row vortex street in the near wake at high amplitudes of oscillation.

The three-dimensional modes that grow on these periodic base flows were investigated using Floquet stability analysis. It was found that the rotational oscillation dramatically suppressed mode B, even for small amplitudes of oscillation. Mode A was also damped, but not as significantly as mode B. This is due to the reduction of wake length scale and the much larger effect of viscous damping at smaller scales. When the double-row wake occurs in the near wake for high rotational oscillation amplitudes, a new three-dimensional transition mode has been identified, which has been dubbed mode D and has the same symmetries as mode A.

REFERENCES

BARKLEY, D. & HENDERSON, R. D. 1996 Three-dimensional Floquet stability analysis of the wake of a circular cylinder. *J. Fluid Mech.* **322**, 215–241.

BARKLEY, D., TUCKERMAN, L. S. & GOLUBITSKY, M. 2000 Bifurcation theory for three-dimensional flow in the wake of a circular cylinder. *Phys. Rev.* E **61** (5), 5247–5252.

BLACKBURN, H. M. & LOPEZ, J. M. 2003 On three-dimensional quasi-periodic Floquet instabilities of two-dimensional bluff body wakes. *Phys. Fluids* **15** (8), L57–L60.

BLACKBURN, H. M., MARQUES, F. & LOPEZ, J. M. 2005 Symmetry breaking of two-dimensional time-periodic wakes. *J. Fluid Mech.* **522**, 395–411.

CANUTO, C., HUSSAINI, M., QUARTERONI, A. & ZANG, T. 1990 *Spectral Methods in Fluid Dynamics*, 2nd edn. Springer.

HENDERSON, R. D. 1997 Nonlinear dynamics and pattern formation in turbulent wake transition. *J. Fluid Mech.* **352**, 65–112.

JOHNSON, S. A., THOMPSON, M. C. & HOURIGAN, K. 2004 Predicted low frequency structures in the wake of elliptical cylinders. *Eur. J. Mech.* B/*Fluids* **23** (1), 229–239.

JULIEN, S., LASHERAS, J. C. & CHOMAZ, J.-M. 2003 Three-dimensional instability and vorticity patterns in the wake of a flat plate. *J. Fluid Mech.* **479**, 155–189.

KARNIADAKIS, G. E., ISRAELI, M. & ORSZAG, S. A. 1991 High-order splitting methods of the incompressible Navier–Stokes equations. *J. Comput. Phys.* **97**, 414–443.

KARNIADAKIS, G. E. & SHERWIN, S. J. 2005 *Spectral/hp Methods for Computational Fluid Dynamics*. Oxford University Press.

KARNIADAKIS, G. E. & TRIANTAFYLLOU, G. S. 1992 Three-dimensional dynamics and transition to turbulence in the wake of bluff objects. *J. Fluid Mech.* **238**, 1–30.

LANDMAN, M. J. & SAFFMAN, P. G. 1987 The three-dimensional instability of strained vortices in a viscous fluid. *Phys. Fluids* **30**, 2339–2342.

LEONTINI, J. S., STEWART, B. E., THOMPSON, M. C. & HOURIGAN, K. 2006 Wake state and energy transitions of an oscillating cylinder at low Reynolds number. *Phys. Fluids* **18**, 067101.

LEONTINI, J. S., THOMPSON, M. C. & HOURIGAN, K. 2007 Three-dimensional transition in the wake of a transversely oscillating cylinder. *J. Fluid Mech.* **577**, 79–104.

LEWEKE, T. & WILLIAMSON, C. H. K. 1998a Cooperative elliptic instability of a vortex pair. *J. Fluid Mech.* **360**, 85–119.

LEWEKE, T. & WILLIAMSON, C. H. K. 1998*b* Three-dimensional instabilities in wake transition. *Eur. J. Mech.* B/*Fluids* **17**, 571–586.

MARQUES, F., LOPEZ, J. M. & BLACKBURN, H. M. 2004 Bifurcations in systems with Z_2 spatio-temporal and O(2) spatial symmetry. *Physica* D **189**, 247–276.

PONCET, P. 2002 Vanishing of mode B in the wake behind a rotationally oscillating circular cylinder. *Phys. Fluids* **16**, 2021–2023.

PROVANSAL, M., MATHIS, C. & BOYER, L. 1987 Bénard–von Kármán instability: transient and forced regimes. *J. Fluid Mech.* **182**, 1–22.

RYAN, K., THOMPSON, M. C. & HOURIGAN, K. 2005 Three-dimensional transition in the wake of bluff elongated cylinders. *J. Fluid Mech.* **538**, 1–29.

SHEARD, G. J., THOMPSON, M. C. & HOURIGAN, K. 2003*a* A coupled Landau model describing the Strouhal–Reynolds number profile of the three-dimensional wake of a circular cylinder. *Phys. Fluids* **15**, L68–L71.

SHEARD, G., THOMPSON, M. C. & HOURIGAN, K 2003*b* From spheres to circular cylinders: the stability and flow structures of bluff ring wakes. *J. Fluid Mech.* **492**, 147–180.

THIRIA, B., GOUJON-DURAND, S. & WESFREID, J. E. 2006 Wake of a cylinder performing rotary oscillations. *J. Fluid Mech.* **560**, 123–147.

THIRIA, B. & WESFREID, J. E. 2007 Stability properties of forced wakes. *J. Fluid Mech.* **579**, 137–161.

THOMPSON, M. C., HOURIGAN, K., CHEUNG, A. & LEWEKE, T. 2006*a* Hydrodynamics of a particle impact on a wall. *Appl. Math. Modelling* **30** (11), 1356–1369.

THOMPSON, M. C., HOURIGAN, K., RYAN, K. & SHEARD, G. J. 2006*b* Wake transition of two-dimensional cylinders and axisymmetric bluff bodies. *J. Fluids Struct.* **22** (6), 793–806.

THOMPSON, M. C., HOURIGAN, K. & SHERIDAN, J. 1996 Three-dimensional instabilities in the wake of a circular cylinder. *Exp. Therm. Fluid Sci.* **12**, 190–196.

THOMPSON, M. C., LEWEKE, T. & WILLIAMSON, C. H. K. 2001 The physical mechanism of transition in bluff body wakes. *J. Fluids Struct.* **15**, 607–616.

WILLIAMSON, C. H. K. 1988 The existence of two stages in the transition to three-dimensionality of a cylinder wake. *Phys. Fluids* **31** (11), 3165–3168.

WILLIAMSON, C. H. K. 1996 Three-dimensional wake transition. *J. Fluid Mech.* **328**, 345–407.

WILLIAMSON, C. H. K. & BROWN, G. L. 1998 A series in $1/\sqrt{(Re)}$ to represent the Strouhal–Reynolds number relationship of the cylinder wake. *J. Fluids Struct.* **12**, 1073–1085.

WILLIAMSON, C. H. K. & PRASAD, A. 1993 A new mechanism for oblique wave resonance in the natural far wake. *J. Fluid Mech.* **256**, 269–313.

WU, J., SHERIDAN, J., WELSH, M. C. & HOURIGAN, K. 1996 Three-dimensional vortex structures in a cylinder wake. *J. Fluid Mech.* **312**, 201–222.